

Surface Treatment of Powder-Bed Fusion Additive Manufactured Metals for Improved Fatigue Life

David B. Witkin, Dhruv N. Patel, Henry Helvajian, Lee Steffeney, and Agustin Diaz

(Submitted March 23, 2018; in revised form August 16, 2018; published online November 19, 2018)

High-cycle fatigue (HCF) tests were conducted on samples fabricated by two powder-bed additive manufacturing techniques. Samples were tested with as-produced surfaces and after various non-contact surface improvement treatments. Ti-6Al-4V samples were made using both electron beam melting (EBM) and selective laser melting (SLM), while Inconel 625 was fabricated using SLM. Ti-6Al-4V was treated with a commercial chemically accelerated vibratory polishing process, with target material removal of approximately 200 μm from each surface for EBM samples and 100 μm for SLM samples. This technique led to increases in both the number of cycles before failure at a given loading condition and endurance limit (at 10^7 cycles) compared to samples with as-produced surfaces. The results are interpreted as the reduction in elastic stress concentration factor associated with surface defects where fatigue cracks initiate. SLM 625 was treated with both an abrasive polishing method and laser surface remelting. Both methods led to improvements in surface roughness, but these did not lead to improvements in fatigue properties of SLM 625. For abrasive polished samples, the combination of improved measured surface roughness without fatigue property enhancement suggests that surface material is removed, but the roots of surface defects, where fatigue cracks initiate, were left intact. For laser treatment, the remelted surface layer retained a rapidly solidified microstructure that did not increase the number of cycles before crack initiation even though the surface was smoother compared to the surface prior to polishing.

Keywords additive manufacturing, dynamic, high cycle fatigue, mechanical, superalloys, surface finish, titanium

1. Introduction

The high-cycle fatigue (HCF) properties of metallic materials made by additive manufacturing (AM) have received considerable recent interest (Ref 1-3). Life-limiting features that influence HCF in metallic specimens made by AM techniques may include internal porosity, near-surface or surface-connected porosity and surface roughness. Fatigue failures are a notable issue for aerospace applications, and as components made by AM are brought into service, new failure modes and their causes need to be identified (Ref 4). Understanding HCF properties of AM materials and how they are influenced by defect populations is just one challenge for industries exploring the potential benefits and trade-offs associated with AM compared to traditional fabrication.

Surveying the expanding literature on fatigue properties of AM materials requires some awareness of the end user's requirements and tolerance for risk. For example, hot isostatic

pressing (HIP) is likely to be employed for many parts entering aerospace service, so studies of test materials that have not been subjected to HIP are not likely to contain microstructures and defect populations characteristic of deployed components. In addition, test methods such as rotating beam fatigue are not endorsed by standard references such as MIL-HDBK-5 (Ref 5) (now known as Metallic Materials Properties Development and Standardization [MMPDS]) and data for AM materials derived from these and other nonstandard test methods will carry some questions for general applicability or use in design and analysis.

If only HIP'ed materials are considered, then fatigue crack initiation is much less likely to occur at internal porosity, which has been found in many studies of non-HIP'ed material, and more likely to occur at surfaces. The influence of surface roughness on fatigue performance has been documented for a range of alloys, including Ti-6Al-4V (Ref 6, 7), austenitic stainless steel 316L and precipitation-hardened stainless steel 15-5 (Ref 8). Comparison of fatigue results for surface features of AM nickel-based superalloy Inconel 625 with the wrought, machined version of the alloy has also been documented (Ref 9). The influence of surface roughness on HCF has been assessed using both empirical (Ref 9, 10) and computational (Ref 11) considerations of elastic stress concentration, and fatigue crack growth threshold due to different sized surface defects based on the Kitagawa-Takahashi diagram (Ref 12).

Because the fatigue performance of AM metals and alloys with as-produced surfaces is generally inferior to machined surfaces (whether compared to either AM or wrought test specimens), AM parts can benefit from improved surfaces. While standard machining is obviously one means to achieve this, extensive post-printing machining erodes the economic value of the AM process. It also limits the design complexity enabled by AM, because if regions subjected to dynamic or cyclic loading conditions must be machined to improve their

This article is an invited paper selected from presentations at the symposium "Additive Manufacturing of Metals: Fatigue and Fracture," held during MS&T17, October 8-12, 2017, in Pittsburgh, PA, and has been expanded from the original presentation.

David B. Witkin, Dhruv N. Patel, Henry Helvajian, and Lee Steffeney, Space Materials Laboratory, The Aerospace Corporation, El Segundo, CA; Agustin Diaz, REM Surface Engineering, Brenham, TX. Contact e-mail: david.b.witkin@aero.org.

fatigue properties, they must also be accessible to machining operations. A similar argument could be made for surface modifications such as shot peening, which relies on the formation of a surface compressive residual stress layer to improve fatigue crack initiation under tensile loads. Nevertheless, a modification of shot peening known as ultrasonic nanocrystalline surface modification (UNSM) that relies on a combination of surface layer grain refinement and residual stress formation through high-frequency surface contact (Ref 13) has been recently shown to improve the rotating beam fatigue performance of SLM Ti-6Al-4V that was not HIP'ed (Ref 14). While not a machining operation involving material removal, UNSM requires contact with the workpiece, and thus, complex geometric forms may not be readily treated by this method.

Non-contact, surface modification methods may be preferable, particularly for those that do not require line-of-sight access for machining tools or shot peening. In this work, we examine the influence of three non-contact surface improvement methods on the fatigue behavior of Ti-6Al-4V made by either selective laser melting (SLM) or electron beam melting (EBM) and Inconel 625 made by SLM. A chemically accelerated vibratory finishing (CAVF) method known as Extreme Isotropic Superfinishing® (ISF®) developed by REM Surface Engineering (Brenham, Texas) was applied to the Ti-6Al-4V specimens. The CAVF process is a tool-less method based on chemical conversion of a thin surface layer that is subsequently removed by contact with vibrating, non-abrasive media (Ref 15, 16). It has been used in conjunction fatigue testing of carburized steel (Ref 17), where it improved fatigue life compared to shot peening, and in low-alloy steel (Ref 18). Its influence on fatigue life is based on surface finish improvement, as it does not significantly alter surface residual stress (Ref 15) or reduces it when applied to shot-peened surfaces (Ref 18).

An abrasive polishing method and laser surface remelting method were used on the Inconel 625. The surface roughness of all treated samples showed significant improvement over that of the as-produced surfaces, but only the CAVF process on Ti-6Al-4V improved the HCF properties. This is interpreted in terms of the elastic stress concentration associated with surface defects under cyclic tensile loads: the addition of chemical action on sharp crack-like features not only improves the overall surface roughness, but also expands and rounds the tips of these features where fatigue cracks are most likely to initiate. Thus, material removal to the full depth of the surface features was not required to show significant improvement in fatigue life.

2. Materials

All AM materials used in this study were purchased from commercial AM service providers. Suppliers were instructed to use their best AM practices in fabricating the test samples, but no special controls or requirements were imposed. Samples were designed to be compliant with requirements found in ASTM E466 (Ref 19) for load-controlled fatigue testing. EBM Ti-6Al-4V flat dog bones (Fig. 1) were purchased from CalRAM, Inc. (Camarillo, California). Specimens were fabricated at CalRAM using Arcam S12 EBM equipment. The gauge section of the specimen as designed was 25.4 mm long,

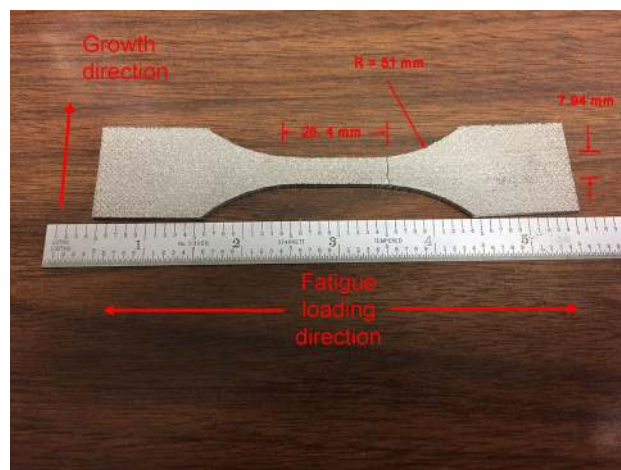


Fig. 1 Photograph of EBM Ti-6Al-4V flat dog bone specimen, with EBM growth and fatigue loading directions indicated

7.94 mm wide and 2.38 mm thick. Transition regions between the gauge and grip sections had a radius of 51 mm. One design consideration was that specimens be fabricated in a horizontal orientation as shown in Fig. 1 without use of build supports, so that testing in the as-built condition could be performed without alteration of the as-produced surface on any face or edge of the test specimen.

SLM test specimens were produced as flat notched specimens ($K_t \sim 3$) as shown in Fig. 2. The main intent of using a notched specimen was to limit the total surface area that needed to be treated with a laser. The Inconel 625 specimens were built at Stratasys Direct Manufacturing (Austin, TX), on edge as shown in Fig. 2. This enabled both top and bottom notches to be built without supports, again allowing comparison of true as-produced surfaces to treated surfaces. The Ti-6Al-4V specimens were built at Incodema3D (Ithaca, New York), but were built flat on the build plate to reduce printing time and specimen cost. Consequently, one side of the specimen had a surface that had been altered by electrical discharge machining (EDM) to remove it from the build plate. In this case, however, the notch root was a vertically oriented wall so the EDM surface on one face is not expected to have significantly impacted fatigue behavior.

All test specimens were HIP'ed by subcontractors to the AM material suppliers, according to the latter's requests. HIP cycles were 900 °C at 100 MPa for 2 h for EBM Ti-6Al-4V, 925 °C and 100 MPa for 3 h for the SLM Ti-6Al-4V and SLM 625 at 1200 °C and 100 MPa for 4 h.

3. Methods

Details of the laser surface remelting procedure have been previously described (Ref 20). In summary, a continuous wave IPG Photonics 200 W laser operating at 1064 nm with a spot size of approximately 30 μm was used to remelt the surface of already heat-treated Inconel 625 specimens. This process was shown to control the depth of the melted surface layer in a uniform fashion. The samples received no heat treatment after laser treatment, so the as-solidified remelted material comprised the outer surface. Remelting layer depth was 100-200 μm .

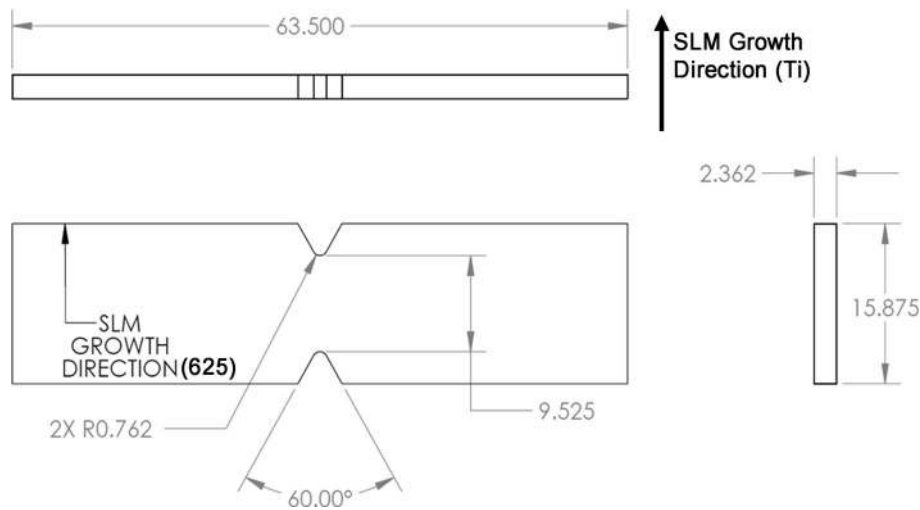


Fig. 2 Design of the notched fatigue specimen with $K_t = 3$ that was used to build SLM Ti-6Al-4V and Inconel 625 specimens (All values are in mm)

CAVF processing was performed on titanium samples, and abrasive finishing of Inconel samples was performed at REM Surface Engineering. The EBM specimens had a higher surface roughness, so the CAVF process was not performed to a specific level of surface roughness, but rather to a total material removal targeted at less than 400 μm for dimensions of interest, or 200 μm on a given surface. Although this did not optimize surface roughness, it was intended to maintain specimen dimensional ratios controlled by ASTM E466 so that comparison of fatigue test results with or without surface finishing would not be compromised by widely different specimen dimensions.

4. Fatigue Testing

All fatigue tests were performed on an Instron servo hydraulic load frame controlled by Instron WaveMatrix software. Specimens were fixed with hydraulic wedge grips. All tests of surfaced treated specimens were run at a stress ratio (R) of 0.1 at a frequency of 20 Hz. For the specific case of EBM Ti-6Al-4V, additional specimens were tested at $R = 0.5$, and those results are included for comparison. Specimen dimensions (thickness and width) were individually measured to determine test loads for a targeted stress.

5. Results

While the primary focus of the investigation was fatigue testing, results are presented for material removal and surface roughness measurements as well.

5.1 Material Removal

Results for material removal via CAVF of Ti-6Al-4V and abrasive polishing of 625 are given in Table 1 and are expressed as average measured specimen dimensions for key dimensions. For surface improvement using material removal, the entire part was treated, although only the reduced sections

are of interest for fatigue testing. Laser surface polishing of metals may involve either removal of material via ablation or reallocation of material via remelting (Ref 21), but in this case laser remelting was limited to the surfaces enveloped by the notches and did not remove material. Any changes in specimen dimensions in the treated areas were within the precision range of the micrometer or calipers used. While material removal is not reported for laser-treated samples, their as-built dimensions are the same as those reported for SLM 625 in Table 1.

Comparison of as-built dimensions with drawing intent shows that SLM specimens of both alloys are within or close to standard drawing tolerances (taken as ± 0.13 or 0.26 mm). In measuring specimen dimensions with a caliper or micrometer, it is important to recognize that sintered metal powder particles or incompletely melted powder contributes to the surface roughness and appearance of powder-bed AM parts. Some of the relatively larger degree of overbuilding in the EBM Ti-6Al-4V compared to SLM alloys may be due in part to the larger powder particle sizes used in the EBM process.

Comparison of the results of material removal in Table 1 for thickness (removal from the faces of specimens) and width (removal from edges) respectively show that they were equal or nearly equal. This is an important consideration for surface improvement of actual parts. Post-finish dimensions show larger deviation from as-designed print dimensions than as-built, falling slightly below drawing intent. Because the specimens were not originally designed or printed anticipating subsequent material removal through surface finishing, it is expected that future efforts will accommodate the surface finishing steps by adding material to the print dimensions. In the present case, however, the overall deviation from design intent in either the as-built or as-polished condition is small enough that fatigue testing is not likely to have been impacted.

5.2 Surface Roughness Measurements

Surface roughness measurements using profilometers are the most obvious way to assess the changes rendered by surface treatment. Surface roughness was measured on samples both before and after surface finish treatments, using OmniSurf profiling software with a 2.5-mm filter. Surface roughness measurements of EBM and SLM Ti-6Al-4V samples before

Table 1 Dimensions of gauge sections of test materials in the as-built and after CAVF processing, along with comparison to designed dimensions

	Measured values, mm							
	Drawing intent		As built		After CAVF		Material removal	
	Thickness	Width	Thickness	Width	Thickness	Width	Thickness	Width
SLM Ti-6Al-4V	2.38	15.88	2.41	15.89	2.19	15.60	0.22	0.29
EBM Ti-6Al-4V	2.38	7.94	2.49	8.19	2.09	7.87	0.40	0.32
SLM 625	2.38	15.88	2.35	15.80	2.27	15.71	0.08	0.09
Deviation from print, mm								
As built					Polished			
Thickness				Width		Thickness		Width
SLM Ti-6Al-4V	0.03		0.01		- 0.19		- 0.28	
EBM Ti-6Al-4V	0.11		0.25		- 0.29		- 0.07	
SLM 625	- 0.03		- 0.08		- 0.11		- 0.17	

Table 2 Surface roughness measurements of EBM and SLM Ti-6Al-4V samples before and after CAVF (all values in μm)

	R_a	R_q	R_v	R_t
EBM Ti-6Al-4V				
Before	19 ± 1	25 ± 2	59 ± 7	160 ± 20
After	13 ± 1	21 ± 2	57 ± 7	91 ± 9
SLM Ti-6Al-4V				
Before	6.5 ± 0.9	8.2 ± 1.5	19 ± 5	40 ± 20
After	0.46 ± 0.04	1.40 ± 0.24	2.42 ± 0.71	14 ± 1

Table 3 Surface roughness measurements of SLM Inconel 625 specimens before and after abrasive polishing (all values in μm)

	R_a	R_q	R_v	R_t
SLM Inconel 625				
Before	5.4 ± 0.3	8.0 ± 0.6	11 ± 2	47 ± 2
After	0.18 ± 0.03	0.64 ± 0.23	1.9 ± 0.5	10 ± 4

and after CAVF for various metrics of surface roughness are given in Table 2 (all values in μm). These values are arithmetic mean roughness (R_a), RMS mean roughness (R_q), maximum valley depth (R_v) and total profile height (R_t). These values are reported to two significant figures and represent measurements at three locations on the pretested specimens. Discussion of the relative merits of these different metrics specifically for surface roughness characterization of AM materials suggests that the most commonly used R_a may not on its own be the most appropriate way to measure and report surface roughness (Ref 22, 23).

Surface roughness of abrasive polishing of SLM 625 alloy is given in Table 3. Surface roughness measurements of laser remelted material have been previously reported (Ref 20). Those previously reported results are not directly comparable to those in Table 3, as those assessments of laser remelting were not conducted on notched fatigue samples. In addition, different measurement equipment was used. Those previous measurements showed reduction in surface roughness R_a from 10.04 to

6.51 μm and R_v from 12.50 to 8.22 μm (Ref 20). For comparison, a laser remelting process applied to SLM 316L stainless steel reported a reduction in R_a from 12 to 1.5 μm using a similar remelting approach to that employed here (Ref 24).

A qualitative means to assess the change in surface roughness is to look at micrographic images of the treated surface. In Fig. 3, a vertical wall of an EBM Ti-6Al-4V flat dog bone specimen is shown before (left) and after CAVF treatment (right). The as-built surface is characterized by nearly uniform coverage of the surface by semi-sintered or partially melted powder particles, along with horizontally oriented textures with spacing of several hundred micrometers, representing the individual melt layers. After CAVF treatment, the powder particles have been completely removed, but some surface topography remains. While the CAVF process is capable of rendering titanium surfaces smoother than that shown in Fig. 3, as previously discussed, a maximum removal depth was imposed to maintain integrity in comparing fatigue results. EBM equipment models developed subsequent to the S12 used to produce these materials may give different results for EBM Ti-6Al-4V surface roughness in both as-built and improved surfaces.

For SLM Ti-6Al-4V, fatigue crack initiation occurs in the vicinity of the notch root. Notched Ti-6Al-4V samples were printed in a flat orientation, so the surface of interest is the vertical wall of the notch itself. Metallographic images in Fig. 4 show polished sections looking down the wall of the notch in tested specimens. Surface features on the as-built surface on the left-hand side are not present in the CAVF surface-treated specimen in the right-hand image.

Figures 5 and 6 show the result of laser remelting and abrasive polishing, respectively, of SLM Inconel 625. Powder particles have again been removed by both processes. The laser remelting process leaves some surface waviness, while the abrasive treatment leads to very smooth surfaces, although some surface depressions remain, as shown in the right-hand image of Fig. 6. A metallographic cross section of a laser remelted surface (Ref 20) (taken from a test article, not a fatigue specimen) is shown in Fig. 7. The remelted layer is characterized by a uniform melting depth and no apparent heat-affected zone in the parent material. Because the sample was HIP'ed prior to laser treatment, the remelted layer has a different microstructure that is characteristic of as-built SLM 625 with no subsequent thermal treatment.

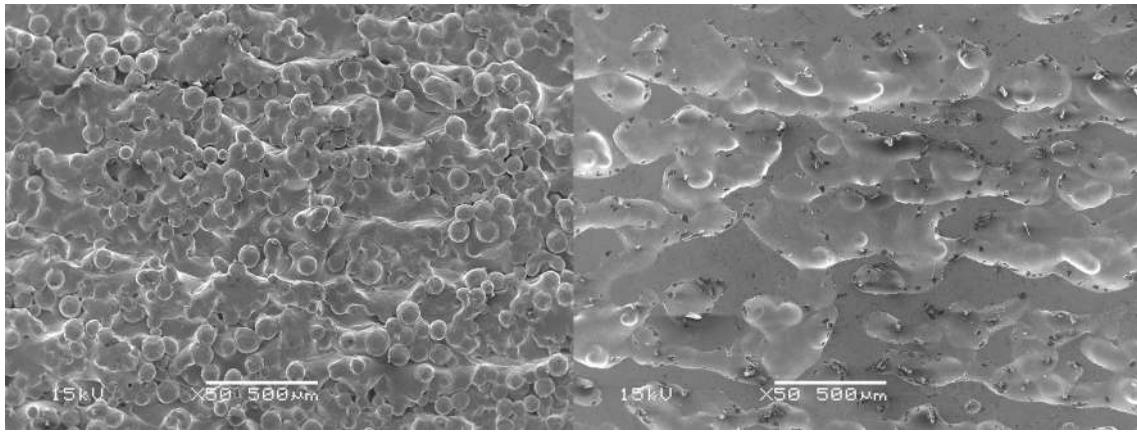


Fig. 3 Scanning electron micrographs of the surface (vertical wall) of EBM Ti-6Al-4V fatigue specimens in the as-built condition (left) and after CAVF treatment (right)



Fig. 4 Optical micrographs of polished and etched cross section of SLM Ti-6Al-4V notch root with as-built surface (left) and after CAVF (right)

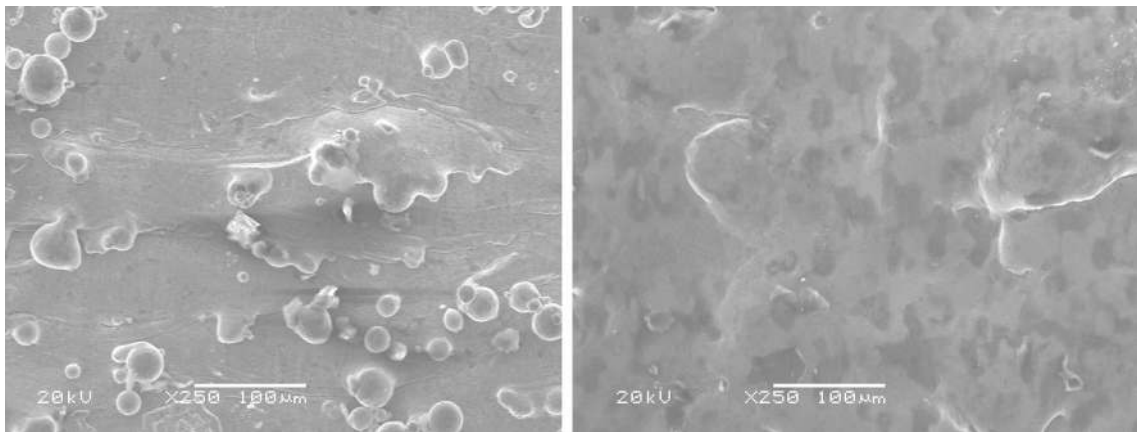


Fig. 5 Scanning electron micrographs of the surface (vertical wall) of SLM Inconel 625 notched fatigue specimen in the as-built condition (left) and after laser remelting (right)

5.3 Fatigue Testing

Fatigue results are presented as S–N plots. In Fig. 8, results are shown for flat EBM Ti-6Al-4V dog bones at $R = 0.1$ and 0.5 with as-produced surfaces and $R = 0.1$ for specimens treated by CAVF. In this plot, one CAVF-treated specimen

tested at a maximum stress of 310 Mpa ($R = 0.1$) did not fail after completing 10 M cycles. This was a much greater number of cycles than another specimen tested at 310 MPa, which failed after approximately 200 K cycles. The sample that did not fail at 310 MPa was retested at a maximum stress of 485 MPa, failing after 82 K cycles. Results at 310 and

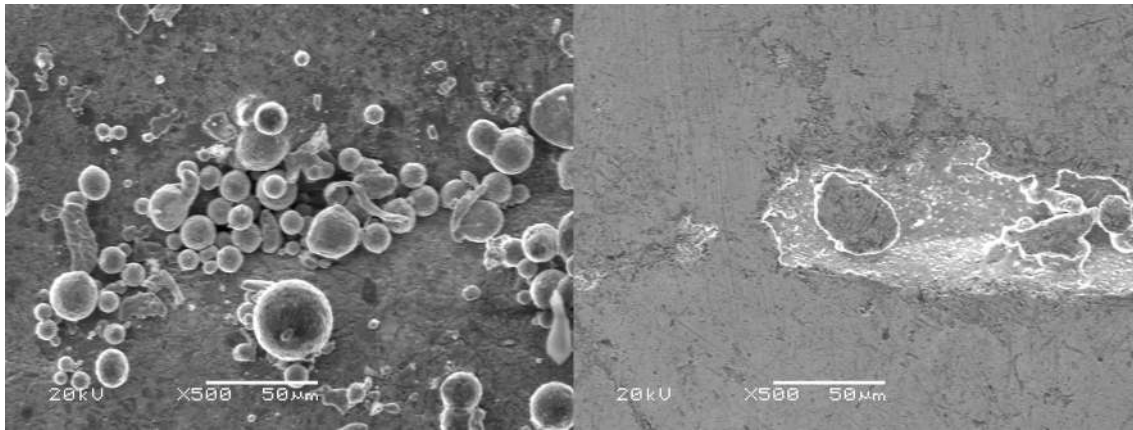


Fig. 6 Scanning electron micrographs of the surface (vertical wall) of SLM Inconel 625 notched fatigue specimen in the as-built condition (left) and after abrasive polishing (right)



Fig. 7 Optical micrograph of a laser remelted layer on a SLM Inconel 625 parent material

485 MPa are seen to be somewhat greater than the rest of the trend described by the treated samples, and subsequent inspection of the fracture surfaces using SEM did not reveal any unusual features in comparison with other EBM Ti-6Al-4V samples that received the same surface treatment.

S-N curves for notched specimens of Ti-6Al-4V made by SLM are shown in Fig. 9, along with models of notched fatigue ($K_t = 2.8$) for annealed Ti-6Al-4V extrusions from MIL-HDBK-5 for comparison. In this case, the CAVF treatment leads to approximate doubling of the number of cycles to failure at a given load. The test run at 205 MPa was halted after 6.7 M cycles. Based on the test results, 205 MPa is estimated as a practical endurance limit for the SLM material in the presence of a notch with $K_t \sim 3$ and $R = 0.1$ after CAVF treatment. The lowest test load for the untreated notched Ti-6Al-4V specimens was 138 MPa, which failed after 428 K cycles. This is too few cycles to estimate the endurance limit for this condition, but given typical characteristics of S-N curves for SLM, EBM and wrought Ti-6Al-4V materials, it is expected that the CAVF treatment would lead to an improvement in endurance limit of 50-100%, or from 100 to 140 MPa to the measured 205 MPa.

The final set of fatigue results is for SLM Inconel 625, as shown in Fig. 10. Included in Fig. 10 are data for vertical round SLM alloy 625 specimens tested at $R = 0.1$ with as-produced surfaces (Ref 9), along with models based on MIL-HDBK-5 data for wrought annealed Inconel 625 tested at $R = 0.1$ for both notched ($K_t = 3$) and unnotched samples. The vertical SLM specimens' fatigue behavior in comparison with these two models was the basis for an estimate that the fatigue behavior of this alloy in SLM form with an as-produced surface could be conceived as roughly equivalent to a notched bar with K_t approximately 2.4-2.8 (Ref 9). The actual notched specimens that are plotted are for horizontally oriented samples with a notch elastic stress concentration factor of 3. The notched samples with as-produced surfaces have S-N curves that are offset from the wrought annealed model with $K_t = 3$ by roughly the same magnitude as the vertical samples are offset from the unnotched wrought annealed material. In this case, however, surface improvement did not lead to any apparent improvement in fatigue behavior. SLM 625 notched samples were split between abrasive surface polishing and laser remelting, and all such samples were tested at either 275 or 310 MPa maximum stress. The results in Fig. 10 for the surface-treated specimens are at best ambiguous, and unlike the results for Ti-6Al-4V, improvement in fatigue performance cannot be inferred.

6. Discussion

The results of high-cycle fatigue testing show that the combination of chemical and vibratory surface finishing (CAVF) led to improvement in the fatigue behavior of Ti-6Al-4V, but that neither abrasive polishing nor laser remelting led to improvement in Inconel 625. The improvement in the fatigue performance after treatment can be considered in several different ways. First, the S-N curve for treated EBM material is approximately coincident with as-produced surface tested at $R = 0.5$ (Fig. 8). The stress ratio in fatigue testing can be considered as a particular ΔK condition; in this case, it is inferred that the effective ΔK at $R = 0.1$ associated with the improved surface has been reduced compared to that of the as-built surface, although it is not implied that the coincidence of the $R = 0.5$ as-built fatigue curve and the $R = 0.1$ CAVF fatigue curve is due to similarity in ΔK . Second, at the lower

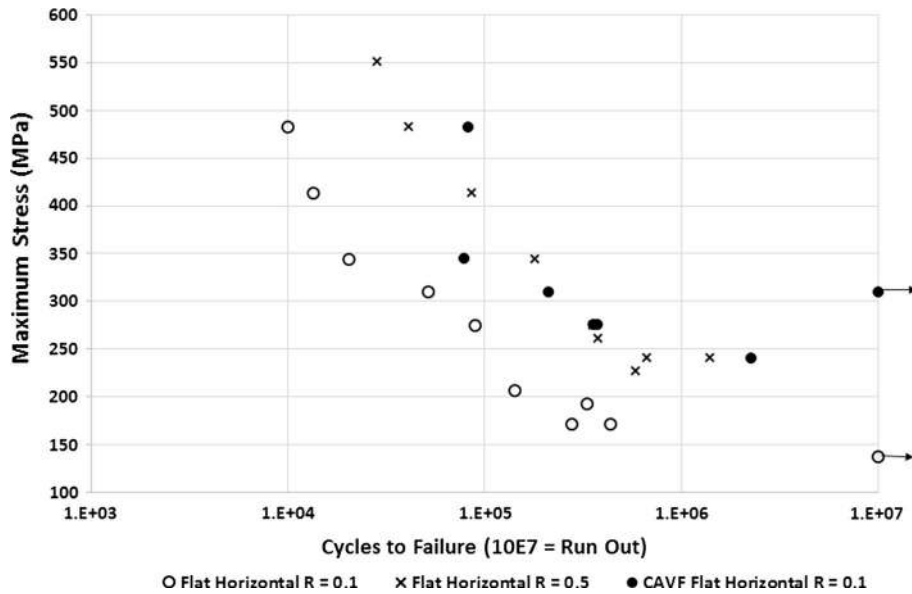


Fig. 8 S–N plot of fatigue results for EBM Ti-6Al-4V. Data points for suspended tests are marked by arrows

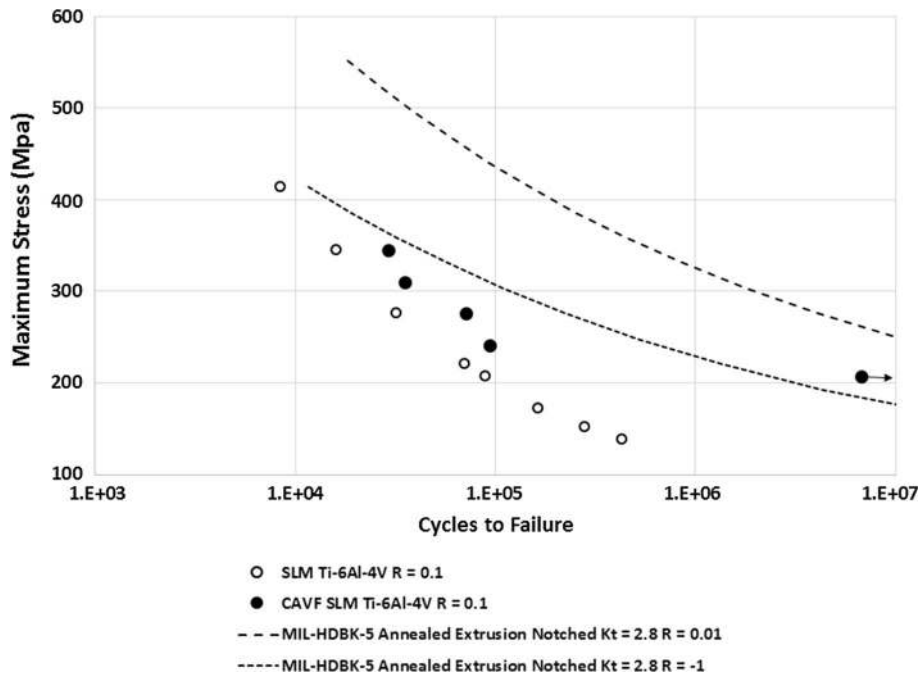


Fig. 9 S–N plot of fatigue results for SLM notched Ti-6Al-4V

lifetime portion of the S–N curves, roughly over the range from 10 K to 300 K cycles before failure, the treated material has a longer fatigue lifetime at the same load levels by a factor of roughly three to five. Finally, if run-out at 10 M cycles is treated as a practical endurance limit, the surface improvement corresponds to an increase in endurance limit from approximately 140 to 280 MPa at $R = 0.1$. In comparison, the approximate endurance limit at the same stress ratio and number of cycles for wrought material is closer to 415 MPa per MIL-HDBK-5 (Ref 5), although the dual-phase microstructures of wrought Ti-6Al-4V are different from AM versions due to the presence of primary alpha phase in the former.

Surface roughness measurements show that all samples showed significant reduction in R_a , which is the most common metric reported for surface roughness. In addition, the CAVF process was not run for sufficient time to remove all surface defects in the EBM Ti-6Al-4V, so that significant surface features remained (Fig. 3). This is particularly evident in specific surface roughness measurements R_q , where the CAVF process led to relatively low reduction, and R_v , where the as-built and treated samples had essentially equivalent values of maximum valley depth. These results raise the question of what aspect of the change in surface finish is responsible for improvement in fatigue performance in the Ti and, conversely,

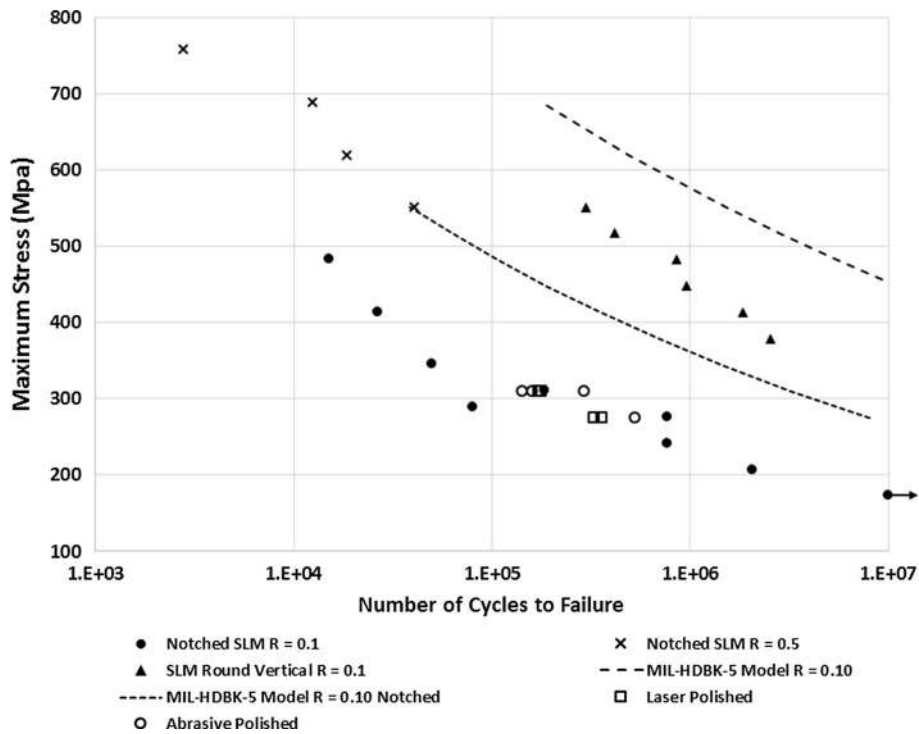


Fig. 10 S–N curve of fatigue results for SLM notched Inconel 625

why fatigue behavior is not affected by a significant change in surface roughness in the nickel alloy.

For the particular case of EBM Ti-6Al-4V, the high roughness, highly irregular surfaces of the as-built and treated EBM samples are measured from non-coincident datums. The abundance of adhered, semi-sintered or partially melted powder particles makes a significant contribution to RMS mean roughness R_q , but the removal of these particles by CAVF reveals surface features that are not probed by a profilometer in the presence of adhered particles. Likewise, maximum valley depth R_v measures two different sets of surface features in the as-built or treated condition. Rather than assuming that the maximum valley depth is unchanged by CAVF, it is more appropriate to conclude that the similarity in R_v for the two conditions is a coincidence because the surface of the specimens has been dramatically changed by the process.

For SLM Ti-6Al-4V, across-the-board improvements in measured surface roughness led to improvements in fatigue life that at first glance are relatively modest by comparison with EBM Ti-6Al-4V. One explanation is that the relatively smoother as-built surfaces of SLM Ti-6Al-4V have essentially less capacity for improvement with respect to HCF properties. The larger relative increase in fatigue life for EBM Ti-6Al-4V after treatment is seen at lower fatigue lifetimes (< 300 K cycles), while design considerations are more likely to be driven by the endurance limit, where the apparent increase after surface treatment is approximately 140 MPa for EBM and on the order of 70–140 MPa for SLM. The latter estimate is similar to that which can be estimated for UNSM surface treatment of un-HIP'ed SLM Ti-6Al-4V in rotating beam fatigue and thus $R = -1$ (Ref 14).

From a practical perspective, increasing the endurance limit by a similar magnitude would imply that the CAVF process has a similar effect for SLM and EBM versions of the alloy. Nevertheless, it is likely that if the CAVF process had been

allowed to proceed in the EBM samples to the same levels of surface roughness of the SLM (Table 2) an even higher endurance limit could have been achieved. The endurance limits of annealed Ti-6Al-4V bar tested at $R = 0.01$ in MIL-HDBK-5 are approximately 485 MPa and 275 MPa for unnotched and notched ($K_t = 2.8$), respectively, giving a fatigue notch factor k_f of 1.75. It remains to be seen whether polishing notched SLM and unnotched EBM Ti-6Al-4V to similar levels of surface roughness could lead to a similar ratio as for annealed bar. The present results put k_f at approximately 1.5 for EBM material that still contains abundant surface defects, so further improvement would raise the value to the point where any intrinsic differences in the fatigue behavior are minimal compared to the macroscopic influence of the elastic stress concentration of the notch.

The surface features that contribute to reduced fatigue lifetimes or endurance limits in as-built specimens can be seen in fracture surfaces of tested fatigue specimens. Fracture surfaces for as-built and CAVF-treated EBM samples are shown in SEM images in Fig. 11. The orientation of the fracture surface in these images is identical to the orientation in which the specimens were printed. This perspective also shows some degree of rounding of the corners of the specimen after the CAVF process, an effect that would not have been accounted for in dimensional measurements, but would also tend to raise the actual stress in the test specimen due to slightly lower cross-sectional area compared to measuring width and thickness and assuming a rectangular cross section.

In all cases, the fatigue crack initiation occurred at the bottom surface of the EBM specimens. In the as-built specimen, the bottom surface is uneven, and unmelted regions can be seen penetrating upward approximately 500 μm into the net section. The surface treatment leads to a more even surface roughness, but as discussed previously by stopping the process after total material removal of 300–400 μm , some of the surface

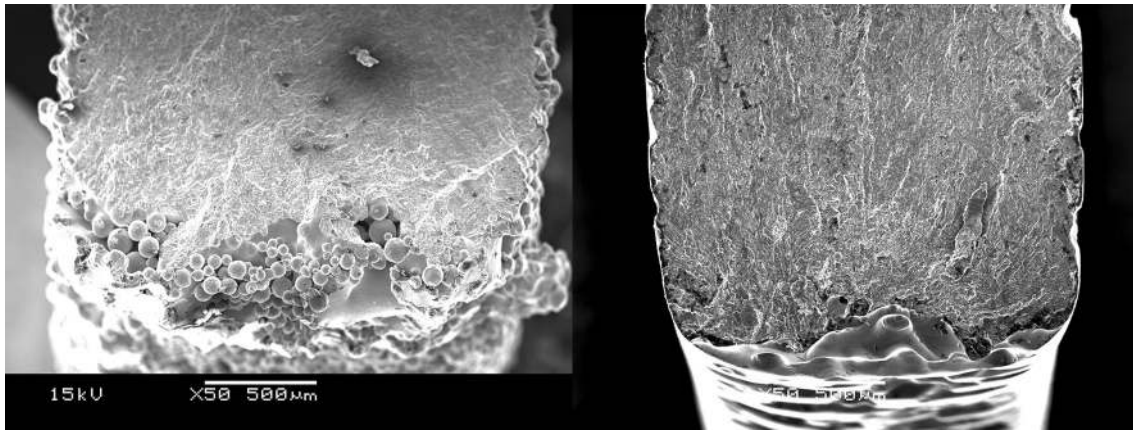


Fig. 11 Fracture surfaces of EBM Ti-6Al-4V fatigue specimens with as-built EBM surface (left) and after CAVF (right)



Fig. 12 Optical micrographs of polished and etched cross sections of EBM Ti-6Al-4V with as-built surface (left) and after CAVF (right). The surfaces shown correspond to unsupported horizontal surfaces facing downward in the vertical direction with respect to the EBM growth direction. The circled feature in the left-hand image is inferred to be typical of high stress concentration where fatigue cracks initiate, and is not present after CAVF treatment

defects are still present, and it is at these types of features where fatigue cracks initiate in the treated samples. It is notable, however, that the interior surface of these flaws has been smoothed and rounded relative to the starting condition. Considering the similarity in R_v for the as-built and treated EBM Ti-6Al-4V (although this was measured on vertical walls, not bottom edges of these samples), the CAVF process is eroding the surface of these surface defects, so the peak depth relative to the sample surface does not change, but the shape of the defect has changed. This is illustrated in metallographic cross sections from the bottom surface of a fatigue specimen in Fig. 12. The circled feature on the left-hand image is a crack-like feature that may have resulted from lack of fusion between adjacent electron beam passes or incomplete melting of powder particles. In the right-hand image, not only has the depth of the surface features been reduced, but this type of fatigue crack starter feature has been removed.

Fracture surfaces of the SLM samples are shown in Fig. 13. The edge of the specimen in the as-built tested specimen is much more even than the EBM Ti-6Al-4V specimen, not only due to intrinsic differences in the two processes but also because of the orientation of the specimens in the printer. In addition, the edge of the fracture surface in the treated specimen shows that defects penetrating the net section are rounder and

their interior surfaces are smoother in comparison with the as-built specimen.

The trends in HCF behavior in the context of surface condition can be understood for all three sets of samples in terms of elastic stress concentration associated with surface defects where fatigue cracks initiate. The elastic stress concentration associated with an elliptical hole can be estimated as (Ref 25):

$$\sigma_y = \frac{\sigma}{2} \left[2 + \frac{2(1 + \beta)}{\alpha^2 - \beta} + \frac{\beta^2 - 1}{\alpha^2 - \beta} \left(1 + \frac{\beta^2 - 13\alpha^2 - \beta}{\alpha^2 - \beta} \right) \right] \quad (\text{Eq 1a})$$

$$\beta = \frac{(a - b)}{(a + b)} \quad (\text{Eq 1b})$$

$$\alpha = \frac{x}{a + b} + \sqrt{\left(\frac{x}{a + b} \right)^2 - \beta} \quad (\text{Eq 1c})$$

In Eq 1a, σ_y is the stress at the edge of an elliptical hole normal to the major axis with length 2a and minor axis length 2b, σ is the net section remotely applied stress normal to the

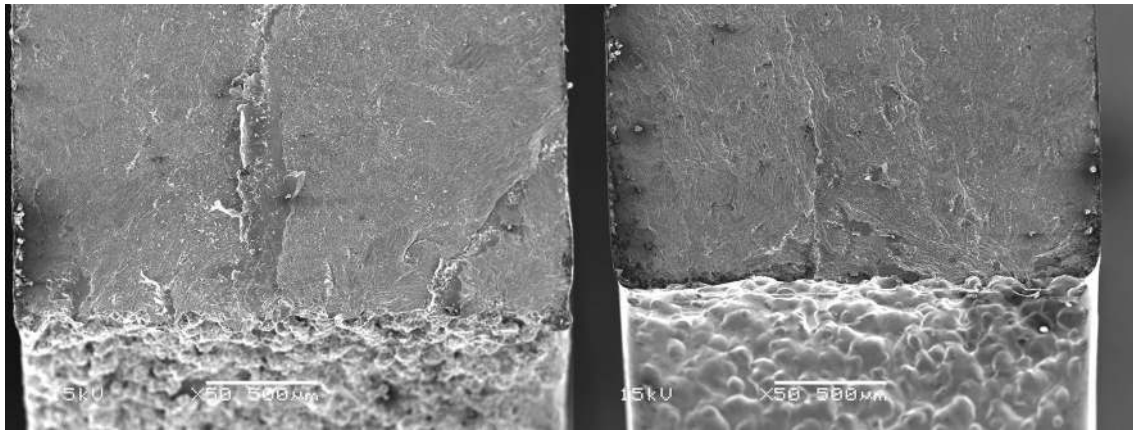


Fig. 13 Fracture surfaces of SLM Ti-6Al-4V fatigue specimens with as-built SLM surface (left) and after CAVF (right)

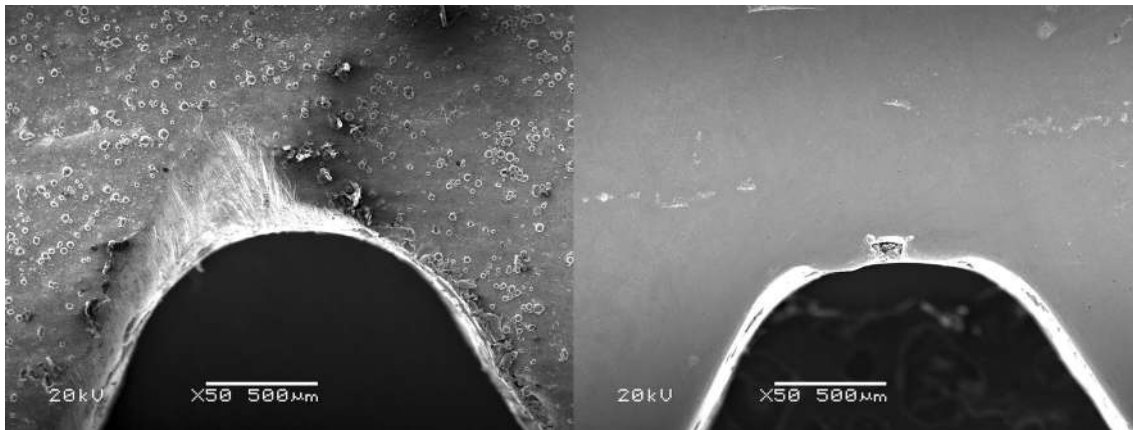


Fig. 14 Scanning electron micrographs of the notch in SLM Inconel 625 specimens in the as-built condition (left) and after abrasive polishing (right). Although the improvement in apparent surface roughness is obvious, the surface feature at the notch root likely responsible for lower fatigue performance compared to wrought or machined specimens is not removed by abrasive polishing

ellipse major axis, and α and β are defined in terms of the ellipse axes and position x from the center of the ellipse normal to the loading direction. In this model, the stress concentration at the end of the hole is the ratio of σ_y to σ . For an ellipse with an aspect ratio (a/b) of 8, the stress concentration is 17; for an aspect ratio of 2, the stress concentration is 5. As a side note, for a circular hole of radius $a/2$, β is 0, α is 1, and the stress concentration is 3.

This approach provides some explanation of why the fatigue performance of the EBM Ti-6Al-4V improves even though there are still surface defects present, as shown in Fig. 3 and 11. The CAVF process may not reduce the deepest penetration of surface features, as seen in R_v , but the combination of mechanical and chemical polishing reduces the stress concentration associated with those defects. The same is true of the SLM Ti-6Al-4V. Although the EBM equipment used to produce these materials (Arcam S12) is no longer considered state of the art for electron beam powder-bed fusion, the general conclusions in terms of the CAVF process used with titanium would be applicable to different surface roughness conditions in more recent vintage equipment.

In the case of SLM Inconel 625, the shortcomings of the abrasive polishing from a fatigue perspective are illustrated by SEM images of the surfaces of notches in as-built and polished specimens that were facing downward vertically during printing

and built without supports (Fig. 14). Downward facing or highly inclined surfaces in powder-bed AM have higher surface roughness than vertical walls, so while the surface roughness of the vertical wall surrounding the notch has been smoothed to sub-micrometer R_a values, the notch root itself shows that a defect is still present. This is a similar outcome of abrasive polishing to that shown in Fig. 6 for a vertical wall, where the roughness due to the adhered powder particles has been removed, but surface defects remain even though measured surface roughness was greatly reduced. Unlike the reduced stress concentration due to CAVF in titanium, the results of abrasive polishing can be considered a reduction in the effective depth of a crack-like surface feature, but not a blunting of its tip. In the case of the elastic stress concentration of a surface notch, small changes in the depth of the notch due to material removal of the surface, while the radius of the notch root is left mostly unchanged, will not lead to significant reductions in K_t (Ref 26; see, for example, Table 6-1, Case 2a, p. 275).

The case of laser polished Inconel 625 is more complicated than that of Ti-6Al-4V. On the one hand, Fig. 5 shows that the surface roughness is decreased by the laser remelting, but that other surface topographic features or asperities are either not fully melted or not removed by the process. SEM images of fracture surfaces of as-built and laser remelted specimens

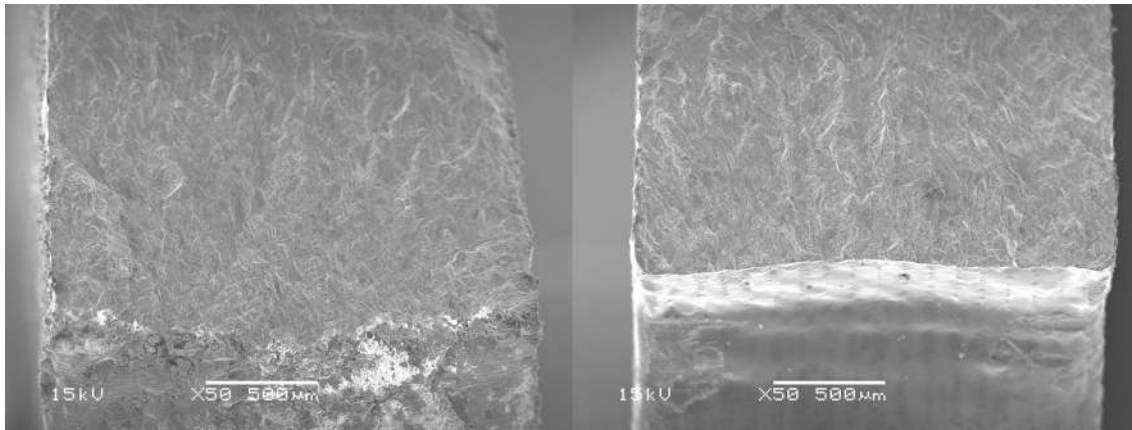


Fig. 15 Fracture surfaces of SLM Inconel 625 notched fatigue specimens with as-built SLM surface (left) and after laser remelting of the notch surface (right)

(Fig. 15) tested at the same stress levels (310 MPa) show considerable improvement in the smoothness of the edge of the notch where fracture initiated. At the same time, the remelted layer shown in Fig. 7 exhibits a rapidly solidified microstructure and an interface with the unmelted parent material, both of which may be more prone to crack initiation even though the outer surface is smoother. The transition from the laser remelted area to the parent material is not seen on fracture surfaces. It is thus not obvious whether the remelted layer is rapidly breached by a fatigue crack at the notch root, meaning that it plays no role in the fatigue of the specimen overall, or if it simply has a similar fatigue crack initiation behavior to the HIP'ed material with an as-produced surface, and is too thin to influence the number of cycles to failure even though its microstructure is different than the bulk material. While the authors are not aware of fatigue testing being performed on SLM specimens subjected to laser polishing, it is likely that a more appropriate approach to future testing will be to perform the polishing step on as-built material, and then HIP the samples so that the entire sample has a uniform microstructure to complement the smoother surface.

7. Conclusions

Surface defects and rough surfaces associated with metallic AM are known to degrade their HCF properties relative to traditional wrought versions of the same alloys and AM materials with machined surfaces. While standard test specimens are relatively straightforward to machine, improved fatigue properties of AM parts require reducing their surface roughness at fatigue sensitive locations that may not be accessible to standard machining operations. Tool-less or non-contact surface finishing as demonstrated here may provide the means to achieve the goal of improving fatigue performance without extensive machining of AM parts.

The results of HCF testing showed unambiguous improvement in the number of cycles to failure and endurance limit for both SLM and EBM Ti-6Al-4V subjected to a chemically accelerated vibratory finishing treatment. At test conditions of $R = 0.1$, the fatigue limit of EBM Ti-6Al-4V was improved by roughly 70 MPa, even though insufficient material was removed to lead to a fully smoothed surface. For SLM Ti-

6Al-4V specimens with a notched design ($K_t = 3$), the improvement in fatigue life is estimated to be between 70 and 140 MPa. In contrast, HCF performance did not improve for SLM Inconel 625 given one of two surface improvement treatments: abrasive polishing or laser remelting.

The fatigue results cannot be explained if only standard surface roughness measurements such as R_a are considered the goal by which the surface treatment is evaluated. For the Ti-6Al-4V, the CAVF process led to improvement in R_a , but also altered the shape of surface flaws that remained after treatment. The improvement in fatigue behavior under these conditions was interpreted as a reduction in elastic stress concentration at locations where fatigue cracks initiated. In the case of EBM Ti-6Al-4V, this explanation can account for the improvement in fatigue life and endurance limit even though measured peak valley depth (R_v) was not changed by the CAVF process. A similar approach based on surface defects leading to fatigue crack initiation could be applied to other materials: Empirical geometric information about these defects obtained from fracture surfaces can be used to assess the influence of fatigue to complement surface roughness measurements that may not necessarily be perceptive of all features of AM surfaces.

For SLM Inconel 625, different processes were used. The lack of improvement in fatigue properties after abrasive polishing is attributed to failure of the process to alter the stress concentration of crack- or notch-like surface features. The abrasive polishing makes these features shallower, but does not alter their interiors, so fatigue life is not increased because the fatigue-limiting features where fatigue cracks initiate have a similar elastic stress concentration or stress intensity after finishing. Nevertheless, the abrasive polishing led to substantial reductions in surface roughness, which could have its own benefits for small holes or channels subjected to fluid flow. Laser remelting appears to eliminate these types of surface features, so the lack of fatigue life enhancement may be due to the microstructure of the remelted layer or other factors.

Acknowledgments

Support for this work was provided in part by the Aerospace Corporation's Independent Research and Development program. We also thank our colleague W. Hansen for development of the laser remelting apparatus and process used to treat the samples. All

service marks, trademarks and trade names are the property of their respective owners.

References

1. S.R. Daniewicz and N. Shamsaei, An Introduction to the Fatigue and Fracture Behavior of Additive Manufactured Parts, *Int. J. Fatigue*, 2017, **94**, p 167
2. P. Li, D.H. Warner, A. Fatemi, and N. Phan, Critical Assessment of Fatigue Performance of Additively Manufactured Ti-6Al-4V and Perspective for Future Research, *Int. J. Fatigue*, 2016, **85**, p 130–143
3. J.J. Lewandowski and M. Seifi, Metal Additive Manufacturing: A Review of Mechanical Properties, *Annu. Rev. Mater. Res.*, 2016, **46**, p 151–186
4. M. Gorelik, Additive Manufacturing in the Context of Structural Integrity, *Int. J. Fatigue*, 2017, **94**, p 168–177
5. United States Department of Defense, Metallic Materials and Elements for Aerospace Vehicle Structures, *Department of Defense Handbook*, United States Department of Defense, Washington, 2003, p 1733
6. D. Greitemeier, C. Dalle Donne, F. Syassen, J. Eufinger, and T. Melz, Effect of Surface Roughness on Fatigue Performance of Additive Manufactured Ti-6Al-4V, *Mater. Sci. Technol.*, 2016, **32**(7), p 629–634
7. K.S. Chan, M. Koike, R.L. Mason, and T. Okabe, Fatigue Life of Titanium Alloys Fabricated by Additive Layer Manufacturing Techniques for Dental Implants, *Metall. Mater. Trans. A*, 2013, **43**(2), p 1010–1022
8. A.B. Spierings, T.L. Starr, and K. Wegener, Fatigue Performance of Additive Manufactured Metallic Parts, *Rapid Prototyping J.*, 2013, **19**(2), p 88–96
9. D.B. Witkin, T.V. Albright, and D.N. Patel, Empirical Approach to Understanding the Fatigue Behavior of Metals Made Using Additive Manufacturing, *Metall. Mater. Trans. A*, 2016, **47**(8), p 3823–3836
10. K.S. Chan, Characterization and Analysis of Surface Notches on Ti-Alloy Plates Fabricated by Additive Manufacturing Techniques, *Surf. Topogr. Metrol. Prop.*, 2015, **3**, p 044006-1–044006-11
11. C.A. Kantzos, R.W. Cunningham, V. Tari, and A.D. Rollett, Characterization of Metal Additive Manufacturing Surfaces Using Synchrotron X-Ray CT and Micromechanical Modeling, *Comput. Mech.*, 2018, **61**(5), p 575–580
12. S. Beretta and S. Romano, A Comparison of Fatigue Strength Sensitivity to Defects for Materials Manufactured by AM or Traditional Processes, *Int. J. Fatigue*, 2017, **94**, p 178–191
13. A. Cherif, Y. Pyoun, and B. Scholtes, Effects of Ultrasonic Nanocrystal Surface Modification (UNSM) on Residual Stress State and Fatigue Strength of AISI, 304, *J. Eng. Mater. Perform.*, 2010, **19**(2), p 282–286
14. H. Zhang, R. Chiang, H. Qin, Z. Ren, X. Hou, D. Lin, G.L. Doll, V.K. Vasudevan, Y. Dong, and C. Ye, The Effects of Ultrasonic Nanocrystal Surface Modification on the Fatigue Performance of 3D-Printed Ti64, *Int. J. Fatigue*, 2017, **103**, p 136–146
15. S. Rao, D. McPherson, and G. Sroka, *Repair of Helicopter Gears*, American Gear Manufacturers Association, Alexandria, 2005, p 11
16. L. Winklemann, O. El Saeed, M. Bell, The Capacity of Superfinished Vehicle Components to Increase Fuel Economy, Part 1, ASME International Design Engineering Technical Conference, Gear Technology, Las Vegas, Nevada, 2009, p 50–60
17. L. Winklemann, M. Michaud, G. Sroka, and A.A. Swiglo, *Impact of Isotropic Superfinishing on Contact and Bending Fatigue of Carburized Steel*, *Advances in Surface Engineering*, SAE International, Las Vegas, 2002, p 13
18. S. Bagherifard, R. Ghelichi, M. Guagliano, and M. Bandini, Effect of REM Finishing on Fatigue Behavior of a Shot Peened Low Alloy Steel, *Key Engineering Materials*, Z. Tonkovic, M.H. Aliabadi, Ed., Trans Tech Publications, Zurich, Switzerland, 2011, p 290–293
19. ASTM, *Standard Practice for Conducting Force Controlled Constant Amplitude Axial Fatigue Tests of Metallic Materials*, ASTM, West Conshohocken, 2007, p 5
20. D.B. Witkin, H. Helvajian, L. Steffaney, and W. Hansen, Laser Post-Processing of Inconel 625 Made by Selective Laser Melting, *Proceedings of the SPIE*, vol. 9738, 2016, p 97380W-1–97380W-10
21. E. Willenborg, Polishing with laser radiation, *Tailored Light 2: Laser Application Technology*, R. Poprawe, Ed., Springer, Berlin, 2011, p 196–202
22. A. Diaz, L. Winkleman, J. Michaud, and C. Terrazas, *Surface Finishing and Characterization of Titanium Additive Manufacturing Components: From Rich to Smooth Surface*, World PM 2016, Hamburg, 2016, p 6
23. T. Grimm, G. Wiora, and G. Witt, Characterization of Typical Surface Effects in Additive Manufacturing with Confocal Microscopy, *Surf. Topogr. Metrol. Prop.*, 2015, **3**, p 12
24. E. Yasa and J.-P. Kruth, Application of Laser Remelting on Selective Laser Melting Parts, *Adv. Prod. Eng. Manag.*, 2011, **6**(4), p 259–270
25. A.-R. Ragab and S.E. Bayoumi, *Engineering Solid Mechanics: Fundamentals and Applications*, CRC Press, Boca Raton, 1999
26. W.D. Pilkey and D.F. Pilkey, *Peterson's Stress Concentration Factors*, Wiley, Hoboken, 2008